Hindawi Publishing Corporation
Mathematical Problems in Engineering
Volume 2014, Article ID 264247, 9 pages
http://dx.doi.org/10.1155/2014/264247

Research Article

Modeling and Analysis of an Air-Breathing Flexible Hypersonic Vehicle

Xi-bin Zhang[1,2] and Qun Zong[2]

[1] *School of Science, Tianjin University of Science and Technology, Tianjin 300222, China*
[2] *College of Electrical Engineering & Automation, Tianjin University, Tianjin 300072, China*

Correspondence should be addressed to Xi-bin Zhang; brookygo@163.com

Received 24 December 2013; Revised 31 March 2014; Accepted 31 March 2014; Published 28 April 2014

Academic Editor: Ricardo Femat

Copyright © 2014 X.-b. Zhang and Q. Zong. This is an open access article distributed under the Creative Commons Attribution License, which permits unrestricted use, distribution, and reproduction in any medium, provided the original work is properly cited.

By using light-weighted material in hypersonic vehicle, the vehicle body can be easily deformed. The mutual couplings in aerodynamics, flexible structure, and propulsion system will bring great challenges for vehicle modeling. In this work, engineering estimated method is used to calculate the aerodynamic forces, moments, and flexible modes to get the physics-based model of an air-breathing flexible hypersonic vehicle. The model, which contains flexible effects and viscous effects, can capture the physical characteristics of high-speed flight. To overcome the analytical intractability of the model, a simplified control-oriented model of the hypersonic vehicle is presented with curve fitting approximations. The control-oriented model can not only reduce the complexity of the model, but also retain aero-flexible structure-propulsion interactions of the physics-based model and can be applied for nonlinear control.

1. Introduction

Hypersonic vehicle (HSV) which can travel faster than 5 times the speed of sound has wide range of applications in military and civilian areas. The research on such vehicle has received tremendous attention in the fields of aeronautics and astronautics in recent years. Unlike conventional aircraft, the propulsion system of hypersonic vehicle is highly integrated into the airframe, which will cause strong couplings between the airframe and propulsion system. Furthermore, high-speed flight, flexible structure, and low natural frequency can result in the bending of fore-body and aft-body of vehicle which will affect the airflow characteristics through the inlet and exit of the engine and hence the aerodynamic layout on the vehicle surfaces. The high couplings among the aerodynamics, flexible structure, and propulsion system make the modeling and control of such vehicle very challenging [1].

From the 1990s, several researchers have paid more attention to the development of the modeling of the hypersonic vehicle. The first attempt at a comprehensive analytical model of a flexible HSV was presented by Chavez et al. Newtonian impact theory was utilized to calculate the forces and moments on the vehicle. The first flexible mode was estimated by a complete NASTRAN analysis, and the couplings between the rigid and flexible dynamic were considered [2]. Clark et al. developed a two-dimensional CFD-based model of a full-scale generic air-breathing hypersonic flight vehicle (CSULA-GHV). The modeling procedure includes configuration design, CFD simulations, and elasticity and aerodynamic interaction [3, 4]. Bolender et al. used a combination of oblique shock, Prandtl-Meyer expansion theory [5], and piston theory [6, 7] to calculate the aerodynamic forces and moments and conducted the first principles model (FPM) with X-43A vehicle geometry. The model is a nonlinear, physics-based model that can capture the couplings among the aerodynamics, flexible structural dynamics, and propulsion system. To overcome the difficulty for controller design, Parker et al. [8], Fiorentini et al. [9], and Sigthorsson et al. [10] presented several control-oriented models by replacing complex aerodynamic force functions in FPM model with curve fitting method, respectively. Frendreis et al. developed a comprehensive aerothermoelastic-propulsion model of a six-degree-of-freedom dynamics of a generic hypersonic vehicle [11, 12]. The three-dimensional model

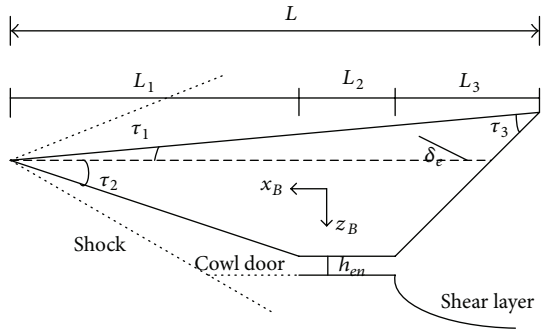

Figure 1: The side view of X-43A HSV.

extends the 3D flight dynamics analysis framework to include the effects of flexibility and unsteady aerodynamics. Based on these models, several studies on the robust guidance and nonlinear control systems design have been published in recent years. The controller design methods provide robust stability and performance for the HSV systems under varying flight conditions [13–17].

The HSV model should contain the real physical characteristics and can be applied for nonlinear control. The unsteady flexible effects, which are omitted in the existing control-oriented models, are significant in aeroservoelasticity analysis. For conducting a high-fidelity control-oriented model which can capture the inherent couplings of vehicle, we concentrate on the influence of flexible effects on the aerodynamic and propulsion system and present an air-breathing flexible HSV model by analyzing the physical characteristics of vehicle flight. Compressible flow theory and Eckert's reference temperature method are used to calculate the complex forces and moments which contain the unsteady flexible effects and viscous effects. By replacing the complicated aerodynamic forces with curve fitting approximations, a simplified control-oriented model is obtained with the interactions of aerodynamics, flexible structure, and propulsion system. The stability analysis and pole-zero analysis are used to analyze the dynamic characteristic of the vehicle model. The results show that the control-oriented model reduces the complexity of the physics-based model and is convenient for nonlinear control.

2. Hypersonic Vehicle Modeling

The hypersonic vehicle, which typically has a tightly integrated airframe and scramjet propulsion system, is quite different from traditional aircraft. Figure 1 shows the side view of X-43A hypersonic vehicle, and the literature [3] presents the detailed parameters of such vehicle. The lower fore-body surface of the vehicle has two functions: one is to produce lift and nose-up pitching moment; another is to act as a compression system to slow the flow velocity and increase the pressure and temperature at the inlet to the engine. The aft-body surface acts as an expansion nozzle to produce lift, thrust, and nose-down pitching moment [2]. The scramjet engine is located underside the vehicle with a translating cowl door, which is used to maintain a shock-on-lip condition for off-design flight conditions [3]. In this vehicle, the airframe and propulsion system cannot separate from each other. Furthermore, the flexible structure bending affects the pressure distribution on the vehicle and the performance of propulsion system. Therefore, the aerodynamic-flexible structure-propulsion interactions should be included in the hypersonic vehicle modeling.

2.1. Flexible Structure. We assume that the fuselage structure is a uniform free-free beam, and the displacements are sufficiently small to satisfy Hooke's Law, and only the transverse displacements of the beam are considered. The assumed modes approach [18] is used to calculate the natural frequencies and mode shapes of the vehicle. This method has the advantage of simplicity and can achieve the desired accuracy. The method is based on Lagrange's equations:

$$\frac{d}{dt}\left(\frac{\partial T}{\partial \dot{q}_i}\right) - \frac{\partial T}{\partial q_i} + \frac{\partial V}{\partial q_i} = f_i, \quad i = 1, 2, \ldots, \tag{1}$$

where T is the total kinetic energy, V is the potential energy of the system, and f_i is the generalized force.

The displacement of the flexible structure is

$$\omega(x,t) = \sum_{i=1}^{n} \Phi_i(x)\,\eta_i(t), \tag{2}$$

where η_i is the generalized model coordinate and the functions $\Phi_i(x)$, $i = 1, 2, \ldots, n$, are the assumed modes which must be linearly independent, satisfy all of the geometric boundary conditions of the flexible structure, and possess all the required derivatives. The free-free beam meets the satisfaction, and we can take the mode shapes of the free-free beam to be the assumed modes.

Calculating the kinetic energy T and potential energy V and substituting them into (1), then, the Lagrange's equations can become

$$M\ddot{\eta} + K\eta = f, \tag{3}$$

where $f = [f_1 \ \cdots \ f_n]$ and the mass matrix $M_{n\times n}$ and the stiffness matrix $K_{n\times n}$ are symmetric.

By setting $f = 0$, $\ddot{\eta} = -\omega^2\eta$, we can get the unforced harmonic dynamics of the system $(\omega^2 I - M^{-1}K)\eta = 0$.

Then the natural frequencies of the flexible structure are the square roots of the eigenvalues of $M^{-1}K$, and the mode shapes are the combinations of the assumed modes $\Phi_i(x)$, $i = 1, 2, \ldots, n$, with the coefficients of the eigenvectors of $M^{-1}K$.

The primary effects of flexible structure on the aerodynamic and propulsion system are in the form of deflections of the fore-body and aft-body as shown in Figure 2, which is a simplification figure of the flexible vehicle model, and only the first flexible mode is considered [3, 7]. Suppose that a bending deflection θ of the beam is sufficiently small; then we can replace the deflection by the deflection angle

$$\theta(x,t) \approx \tan\theta(x,t) = \frac{\partial \omega(x,t)}{\partial x}. \tag{4}$$

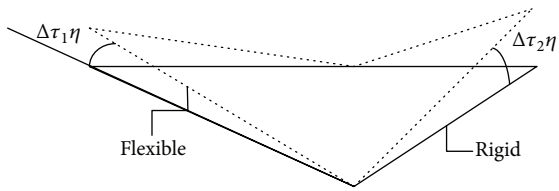

Figure 2: The flexible vehicle model.

By using the principle of separation of variables, we obtain the deflection caused by the ith flexible mode

$$\theta_i(x,t) = \frac{\partial}{\partial x}\left[\varphi_i(x)\,\eta_i(t)\right] = \frac{d\varphi_i(x)}{dx}\eta_i(t), \tag{5}$$

where $\varphi_i(x)$ is the mode shape and $\eta_i(t)$ is the generalized coordinate.

Considering n flexible modes, the fore-body deflection can be written as

$$\Delta\tau_1 = \sum_{i=1}^{n} \frac{d\varphi_i(x)}{dx}\bigg|_{x=0}\eta_i(t). \tag{6}$$

The aft-body deflection is

$$\Delta\tau_2 = \sum_{i=1}^{n} \frac{d\varphi_i(x)}{dx}\bigg|_{x=L}\eta_i(t). \tag{7}$$

Bending of the fore-body and aft-body together can change the airflow characteristics of vehicle surfaces; then it will affect the engine inlet condition and alter the aerodynamic performance.

2.2. Aerodynamic Model. Aerodynamic modeling is an important issue in hypersonic vehicle modeling. The couplings between the flexible dynamics and rigid dynamics always occur through the aerodynamic forces and moments. Oblique shock relations, Prandtl-Meyer theory, and piston theory can be employed to estimate the aerodynamic forces and moments on the vehicle.

2.2.1. Aerodynamic Forces. Shock and expansion waves are common physical phenomena in hypersonic flows. By using the oblique shock and Prandtl-Meyer theory, we can calculate the pressure, Mach number, and temperature behind the shock or expansion wave [3]. Furthermore, the flexible effects affect the wave structure on the vehicle surface and can change the angle of attack and control angles, which in turn change the pressures on vehicle surfaces.

For the upper surface, if $\alpha + \Delta\tau_1 < \tau_1$, an oblique shock wave forms on the upper surface; if $\alpha+\Delta\tau_1 > \tau_1$, an expansion fan forms on the upper surface; if $\alpha + \Delta\tau_1 = \tau_1$, then the upper surface experiences the freestream. By using oblique shock and Prandtl-Meyer theory, we can obtain the force and moment on the upper surface, which can be resolved into x- and z-body axes components:

$$\begin{aligned} F_{x,\mathrm{up}} &= -p_{\mathrm{up}} L \tan\tau_1, \\ F_{z,\mathrm{up}} &= p_{\mathrm{up}} L, \\ M_{\mathrm{up}} &= z_{\mathrm{up}} F_{x,\mathrm{up}} - x_{\mathrm{up}} F_{z,\mathrm{up}}. \end{aligned} \tag{8}$$

Similar to the upper surface of the vehicle, the forces and moments on the lower fore-body surface, engine nacelle, and elevator surface can be obtained, respectively. The pressure over the aft-body surface is affected by the exhaust gases from the propulsion system. By calculating the lower fore-body surface pressure, the inner pressure in the engine and the position of the shear layer, we can get the force and moment on the aft-body surface [2]. Then the resultant aerodynamic forces and moments on the x- and z-body axes F_{xr}, F_{zr}, M_r are summarized from the individual components.

2.2.2. Unsteady Flexible Effects. When traveling at high speed, the interactions between the fluid and the flexible structure of such vehicle may lead to unsteady aerodynamic effects. Understanding the consequences of unsteady aerodynamic caused by flexible effects is significant to the development of flexible vehicle modeling.

Assuming that the flexible effects only occur in the z-direction and the engine is rigid, the unsteady flexible effects here are considered as small perturbations of deformation velocity and angular rate:

$$\dot{\omega}(x,t) = \sum_{i=1}^{\infty} \varphi_i(x)\,\dot{\eta}_i(t) = \Phi\cdot\dot{\eta}, \tag{9}$$

$$\dot{\theta} = \sum_{i=1}^{n} \frac{d\varphi_i(x)}{dx}\dot{\eta}_i(t) = \dot{\Phi}\cdot\dot{\eta}. \tag{10}$$

Piston theory is applied to compute the unsteady aerodynamic effects behind oblique shock waves and expansion fans. The pressure on the surface is given by [7]

$$\frac{P}{P_i} = \left(1 + \frac{\gamma-1}{2}\frac{w_i}{a_i}\right)^{2\gamma/(\gamma-1)}. \tag{11}$$

According to the first-order linear piston theory, the infinitesimal force due to the pressure is

$$dF = -PdAn = -\left(P_i + \rho_i a_i\left[V_i\cdot n\right]\right)dAn, \tag{12}$$

where P_i is the local pressure behind the shock or expansion wave, V_i is the velocity of the surface to the steady flow, ρ_i, a_i are the atmospheric density and sonic speed, respectively, n is the outward pointing surface normal, and dA is the surface element.

For the upper surface, the velocity due to the flexible deformation velocity and angular rate perturbations is

$$V_{\mathrm{up}} = V_1\cos\tau_1\overrightarrow{i} + \left(V_1\sin\tau_1 + \dot{\omega}(x,t)\right)\overrightarrow{k} + \left(\dot{\Phi}\cdot\dot{\eta}\right)\times r_{\mathrm{up}}, \tag{13}$$

where V_1, r_{up} are the velocity of the flow and the position vector of a point on the upper surface, respectively.

Substituting the velocity V_{up} into (12), the unsteady force and moment on the upper surface can be written as

$$\begin{aligned}
\Delta F_{\text{up},x} &= \int_0^L \rho_{\text{up}} a_{\text{up}} \left[\left(\dot{\Phi}\cdot\dot{\eta}\right)\left(x\tan\tau_1^2 - x\right) + \Phi\cdot\dot{\eta}\right]\sin\tau_1\, dx,\\
\Delta F_{\text{up},z} &= -\int_0^L \rho_{\text{up}} a_{\text{up}} \left[\left(\dot{\Phi}\cdot\dot{\eta}\right)\left(x\tan\tau_1^2 - x\right)\right.\\
&\qquad \left. +\Phi\cdot\dot{\eta}\right]\cos\tau_1\, dx,\\
\Delta M_{\text{up}} &= z_{\text{up}}\Delta F_{\text{up},x} - x_{\text{up}}\Delta F_{\text{up},z}.
\end{aligned} \tag{14}$$

For the lower fore-body surface, the unsteady force and moment are given by

$$\begin{aligned}
\Delta F_{df,x} &= \int_0^{L_1} \rho_{df}\alpha_{df} \left[\left(\dot{\Phi}\cdot\dot{\eta}\right)\left(x\tan\tau_2^2 - x\right)\right.\\
&\qquad \left. +\Phi\cdot\dot{\eta}\right]\sin\tau_2\, dx,\\
\Delta F_{df,z} &= \int_0^{L_1} \rho_{df}\alpha_{df} \left[\left(\dot{\Phi}\cdot\dot{\eta}\right)\left(x\tan\tau_2^2 - x\right)\right.\\
&\qquad \left. +\Phi\cdot\dot{\eta}\right]\cos\tau_2\, dx,\\
\Delta M_{df} &= z_{df}\Delta F_{df,x} - x_{df}\Delta F_{df,z}.
\end{aligned} \tag{15}$$

For the lower aft-body surface, the unsteady force and moment are given by

$$\begin{aligned}
\Delta F_{da,x} &= \int_{L_1+L_2}^{L} \rho_{da} a_{da}\\
&\qquad \times \left\{\dot{\Phi}\cdot\dot{\eta}\left[(L-x)\tan\left(\tau_1+\tau_3\right) - L\tan\tau_1\right]\right.\\
&\qquad \times \sin\left(\tau_1+\tau_3\right) + \left(-\left(\dot{\Phi}\cdot\dot{\eta}\right)x + \Phi\cdot\dot{\eta}\right)\\
&\qquad \left.\times\ \sin\left(\tau_1+\tau_3\right)\right\} dx,\\
\Delta F_{da,z} &= -\int_{L_1+L_2}^{L} \rho_{da} a_{da}\\
&\qquad \times \left\{\dot{\Phi}\cdot\dot{\eta}\left[(L-x)\tan\left(\tau_1+\tau_3\right) - L\tan\tau_1\right]\right.\\
&\qquad \times \sin\left(\tau_1+\tau_3\right) + \left(-\left(\dot{\Phi}\cdot\dot{\eta}\right)x + \Phi\cdot\dot{\eta}\right)\\
&\qquad \left.\times\ \cos\left(\tau_1+\tau_3\right)\right\} dx,\\
\Delta M_{da} &= -z_{da}\Delta F_{da,x} - x_{da}\Delta F_{da,z}.
\end{aligned} \tag{16}$$

Summarize the unsteady forces and moments on each surface and denote $F_{x,\text{fle}}, F_{z,\text{fle}}, M_{\text{fle}}$ as the unsteady flexible aerodynamic of vehicle; then we can get the total body force and moment:

$$\begin{aligned}
F_x &= F_{xr} + F_{x,\text{fle}},\\
F_z &= F_{zr} + F_{z,\text{fle}},\\
M &= M_r + M_{\text{fle}}.
\end{aligned} \tag{17}$$

2.2.3. Viscous Effects. The inviscid flow cannot describe the real airflow characteristics. With high Mach flight, the viscous fluid moves relatively to the vehicle which can generate viscous friction, and can result in boundary layer effect and aerodynamic heating. The flow temperature changes and it is difficult to calculate the aerodynamic parameters inside the boundary layer. Similar to the literature [19], Eckert's reference temperature method is used to compute the viscous skin friction on each surface of the vehicle. The reference temperature which is a function of the Mach number (M) and temperature (T) at the edge of the boundary layer as well as the wall (skin) temperature T_w can be written as

$$T^* = T\left[1 + M^2 + 0.58\left(\frac{T_w}{T} - 1\right)\right]. \tag{18}$$

Based on the reference temperature, we can calculate the density ρ^*, the viscosity μ^*, Reynolds number Re^*, and the skin friction coefficient C_f with the perfect gas law and Sutherland's formula. Then, the shear stress on the surface can be computed by

$$\tau_w = \left(\frac{1}{2}\rho_\infty V_\infty^2\right) C_f. \tag{19}$$

Integrating (19), the skin friction drag can be given by

$$F_{\text{vis}} = \int \tau_w\, dx. \tag{20}$$

Then the normal and axial forces are obtained as follows:

$$N_{\text{vis}} = F_{\text{vis}}\sin\beta, \qquad A_{\text{vis}} = F_{\text{vis}}\cos\beta, \tag{21}$$

where β is the surface inclination to the body axis.

By using the coordinate transformation, the additional lift, drag, and moment of viscous effects can be written as

$$\begin{aligned}
L_{\text{vis}} &= N_{\text{vis}}\cos\alpha - A_{\text{vis}}\sin\alpha,\\
D_{\text{vis}} &= N_{\text{vis}}\sin\alpha - A_{\text{vis}}\cos\alpha,\\
M_{\text{vis}} &= N_{\text{vis}}x + A_{\text{vis}}z.
\end{aligned} \tag{22}$$

We consider the viscous skin friction on the upper surface, lower fore-body surface, lower aft-body surface, surface below the engine nacelle, and control surfaces. By calculating the additional lift, drag, and moment on each surface, we can get the total additional lift L_{vis}, additional drag D_{vis}, and additional moment M_{vis}.

Translating the force F_x, F_z into the lift and drag acting on the vehicle and taking the viscous effects into account, the total lift, drag, and pitching moment are

$$\begin{aligned}
L &= F_x\sin\alpha - F_z\cos\alpha + L_{\text{vis}},\\
D &= -F_x\cos\alpha - F_z\sin\alpha + D_{\text{vis}},\\
M &= M_r + M_{\text{fle}} + M_{\text{vis}}.
\end{aligned} \tag{23}$$

The flexible and viscous effects are included in force and moment formulations in (23). If we assume a rigid structure such that $\eta_1 = \eta_2 = \eta_3 = \dot{\eta}_1 = \dot{\eta}_2 = \dot{\eta}_3 = 0$ and viscous effect is excluded, then (23) is steady aerodynamic forces of a rigid body vehicle.

2.2.4. Generalized Forces. In this paper, we present the loadings on the upper surface, lower surface, and control surface; the generalized forces for the first three flexible modes can be written as

$$N_i = \int_0^L \varphi_i(x)\, p_{\text{up}}\, dx - \int_0^{L_f} \varphi_i(x)\, p_{df}\, dx - \int_{L_f+L_n}^{L} \varphi_i(x)\, p_{da}\, dx - \int_{L_f}^{L_n} \varphi_i(x)\, p_{en}\, dx + \varphi_i(x_e)\, F_e, \quad i = 1, 2, 3, \tag{24}$$

where p_{up}, p_{df}, p_{da}, p_{en} are the pressures on the upper surface, lower fore-body surface, engine nacelle, and lower aft-body surface, respectively. F_e is the force act on the elevator surface; $\varphi_i(x)$ is the mode shape, which is calculated by the assumed mode method.

2.3. Thrust. Similar to the literature [20], the scramjet engine consists of 3 sections: a diffuser, a combustor, and an internal nozzle. We assume that the airflow into the engine is parallel to the direction of the body axis. By avoiding the mass flow impinges at the inlet, a translating cowl door is added to increase the mass flow through the engine module. With quasi-one-dimensional aero/thermoanalysis of the flow in the propulsion system and the momentum theorem, the thrust is given by

$$T = \dot{m}_a (V_e - V_\infty) + (p_e - p_\infty) \frac{A_e}{b}, \tag{25}$$

where $\dot{m}_a$ is the air mass flow through the engine, $\dot{m}_a$ is dependent on the fore-body deflection $\Delta\tau_1$, angle of attack α, and the freestream, V_e and p_e are the airflow velocity and pressure at the engine exit, respectively, V_∞ is the freestream airflow velocity, and A_e/b is the exit area per unit width.

2.4. Equations of Motion. Assume that the earth is flat and the fuselage is free-free beam. The equations of motion of the longitudinal dynamics for the hypersonic vehicle based on Lagrange's equations are presented in [3]. By ignoring the weak inertial coupling terms, the flexible mode shapes are orthogonal to the rigid body rotation, which decouples the flexible modes and the rigid body modes, and the couplings between the rigid and flexible modes are included in the aerodynamic forces and moments. Then the simplified longitudinal dynamics of a flexible vehicle written in the stability axis coordinate system are [8, 10]

$$\dot{V} = \frac{1}{m}(T\cos\alpha - D) - g\sin(\theta - \alpha),$$

$$\dot{\alpha} = \frac{1}{mV}(-T\sin\alpha - L) + Q + \frac{g}{V}\cos(\theta - \alpha),$$

$$\dot{q} = \frac{I_{yy}}{M},$$

$$\dot{\theta} = q,$$

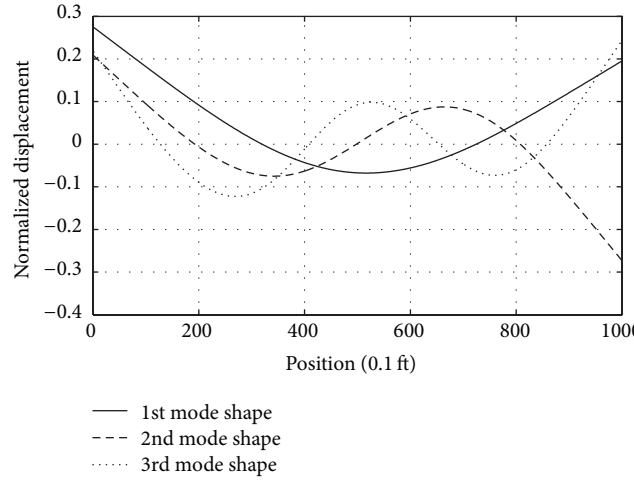

Figure 3: The mode shapes of the flexible structure.

$$\dot{h} = V\sin(\theta - \alpha),$$
$$\ddot{\eta}_i + 2\zeta_i\omega_i\dot{\eta}_i + \omega_i^2\eta_i = N_i, \quad i = 1, 2, 3, \tag{26}$$

where the rigid body states are $\{V, \alpha, q, \theta, h\}$, in which V, α, q, θ, h are the vehicle speed, angle of attack, pitch rate, pitch acceleration, and height, respectively. The flexible states are $\{\eta_1, \dot{\eta}_1, \eta_2, \dot{\eta}_2, \eta_3, \dot{\eta}_3\}$, ζ is the structure damping, ω_i is the frequency, and η_i is the generalized coordinate. The control input elevator deflection δ_e, throttle ϕ, and the couplings between the rigid and flexible modes will appear explicitly in the forces and moment L, D, T, M, N_i which are calculated in the above sections.

3. Control-Oriented Modeling

3.1. Flexible Modes. The natural frequencies of the flexible structure are the square roots of the eigenvalues of $M^{-1}K$; by using the assumed modes method in Section 2.1, we obtain the first three natural frequencies:

$$\omega_1 = 19.7437\ \text{rad/s}, \quad \omega_2 = 47.7851\ \text{rad/s}, \quad \omega_3 = 94.8203\ \text{rad/s}. \tag{27}$$

The first three mode shapes are shown in Figure 3; the deflections of the fore-body and aft-body are presented by

$$\Delta\tau_1 = \Phi_1(\eta_1 \ \ \eta_2 \ \ \eta_3)^T, \quad \Delta\tau_2 = \Phi_2(\eta_1 \ \ \eta_2 \ \ \eta_3)^T, \tag{28}$$

where $\Phi_1 = (\varphi_1'(0), \varphi_2'(0), \varphi_3'(0))$ and $\Phi_2 = (\varphi_1'(L), \varphi_2'(L), \varphi_3'(L))$.

We assume that the generalized coordinates are constant; then $\Delta\tau_1 = -2.3835$ deg, $\Delta\tau_2 = 0.7047$ deg. It can be seen that the fore-body deflection is changed significantly compared to the aft-body deflection.

3.2. Flexible and Viscous Effects. For analyzing the contributions of flexible and viscous effects to the aerodynamic, we

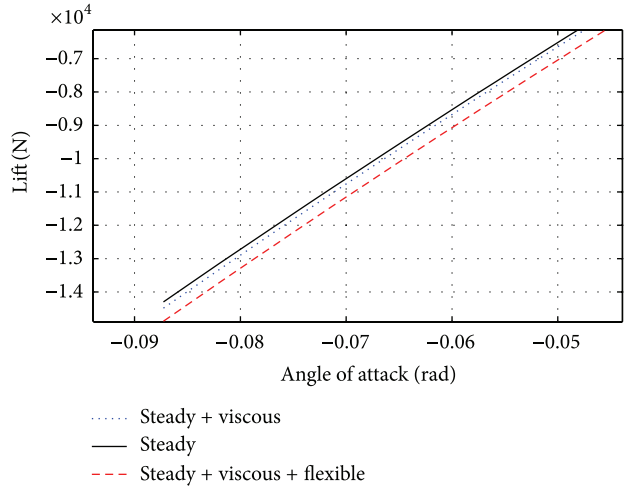

Figure 4: The trend of lift with AOA.

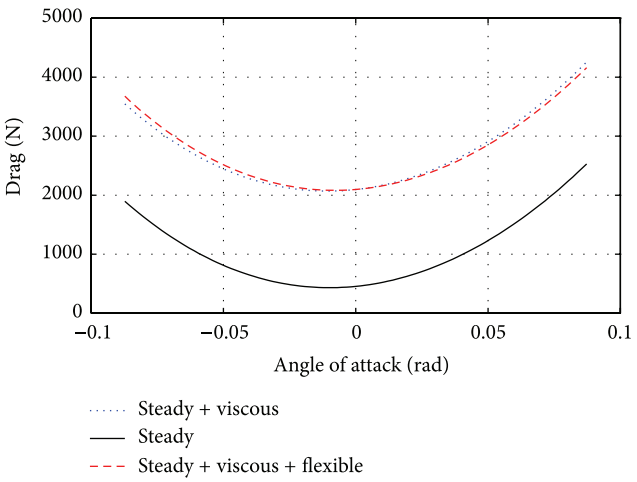

Figure 5: The trend of drag with AOA.

observe the trend of forces with angle of attack and other variables frozen at certain conditions. From Figures 4 and 5, we can see that the viscous drag is large compared to the lift. This is because the viscous forces act parallel to the surface and there is an increase in the drag acting on the vehicle. On the other hand, the flexible effects are relatively small compared to the viscous effects.

We can conclude that the viscous effects are significant contributor to the drag and should be included in the aerodynamic modeling. The flexible effects do not make significant contribution to the forces but cannot be ignored here because the lowest frequency will change with the aerodynamic heating and mass decreasing [17] and will be close to the rigid modes, which can bring the coupling between the rigid and flexible dynamic [21].

Figure 6 shows the trend of thrust with the fore-body deflection. The thrust decreases as the fore-body deflection increases; this is because the bending of vehicle body can result in not enough airflow flown into the engine, which will then affect the propulsion system.

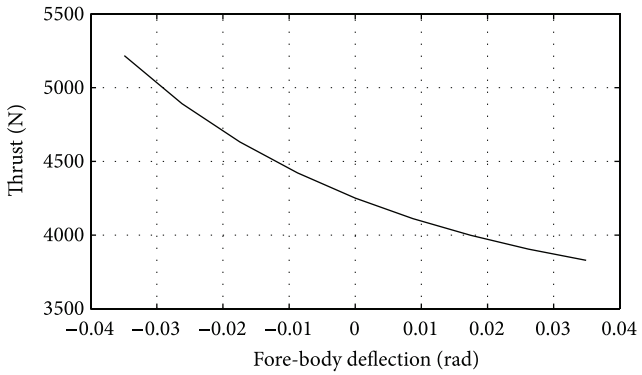

Figure 6: Thrust versus $\Delta\tau_1$.

3.3. Control-Oriented Model. The model in Section 2 captures interactions among the aerodynamics, structural dynamics, and propulsion of the hypersonic vehicle and the strong couplings between the rigid and flexible modes result in intractable systems for nonlinear control. By replacing complex force and moment functions with curve fitting approximations, neglecting certain weak couplings, a simplified control-oriented model can be obtained. The model should be simple enough to facilitate controller design and capture the inherent features which are included in physics-based model. By analyzing the couplings from the aerodynamic data of the model, we choose the variables and the functions of forces and moments which are

$$\begin{aligned} L &\approx \bar{q}SC_L\left(Ma, \alpha, \delta_e, \eta, \dot{\eta}\right), \\ D &\approx \bar{q}SC_D\left(Ma, \alpha, \delta_e, \eta, \dot{\eta}\right), \\ T &\approx \bar{q}SC_T\left(Ma, \alpha, \phi, \delta_e, \eta, \dot{\eta}\right), \\ M &\approx z_T T + \overline{qc}SC_M\left(Ma, \alpha, \delta_e, \eta, \dot{\eta}\right), \\ N_i &\approx \bar{q}SC_{N_i}\left(Ma, \alpha, \delta_e, \eta, \dot{\eta}\right), \quad i = 1, 2, 3, \end{aligned} \tag{29}$$

where $\eta = (\eta_1, \eta_2, \eta_3)$ and $\dot{\eta} = (\dot{\eta}_1, \dot{\eta}_2, \dot{\eta}_3)$ reflect the unsteady effects on the aerodynamic forces and moments.

Based on the aerodynamic data from the physics-based model, we can get the forces and moments coefficients by using the curve fitting method:

$$\begin{aligned} C_L &= C_L^{Ma} Ma + C_L^{\alpha}\alpha + C_L^{\delta_e}\delta_e + C_L^{\eta_1}\eta_1 + C_L^{\eta_3}\eta_3 + C_L^{\dot{\eta}_2}\dot{\eta}_2 + C_L^0, \\ C_D &= C_D^{Ma} Ma + C_D^{\alpha}\alpha + C_D^{\delta_e}\delta_e + C_D^{\eta_1}\eta_1 \\ &\quad + C_D^{\eta_3}\eta_3 + C_D^{Ma\alpha} Ma\cdot\alpha + C_D^{Ma\delta_e} Ma\cdot\delta_e \\ &\quad + C_D^{\alpha\delta_e}\alpha\cdot\delta_e + C_D^{\alpha^2}\alpha^2 + C_D^{\delta_e^2}\delta_e^2 + C_D^o, \\ C_T &= C_T^{Ma} Ma + C_T^{\alpha}\alpha + C_T^{\phi}\phi + C_T^{\alpha^3\phi}\alpha^3\phi \\ &\quad + C_T^{\alpha^2\phi}\alpha^2\phi + C_T^{\alpha\phi}\alpha\cdot\phi + C_T^{Ma\phi} Ma\cdot\phi \\ &\quad + C_T^{\eta_1}\eta_1 + C_T^{\eta_2}\eta_2 + C_T^{\eta_3}\eta_3 + C_T^o, \end{aligned}$$

Table 1: The range of the variables.

Variables	Range	Variables	Range
V (ft/s)	7500~11000	η_2	−0.03~0.04
α (deg)	−5~5	η_3	−0.003~0.004
δ_e (deg)	−10~10	$\dot{\eta}_1$	−3~4
ϕ	0.05~1.5	$\dot{\eta}_2$	−0.3~0.4
η_1	−0.3~0.4	$\dot{\eta}_3$	−0.03~0.04

Table 2: The coefficients of fits for the lift.

Terms	Values	Terms	Values
C_L^{Ma}	−0.00578253	$C_L^{\eta_3}$	−0.0954033
C_L^{α}	5.84425	$C_L^{\dot{\eta}_2}$	−0.00413381
$C_L^{\delta_e}$	0.755975	C_L^{0}	0.0621356
$C_L^{\eta_1}$	−0.0522466		

Table 3: The coefficients of fits for the drag.

Terms	Values	Terms	Values
C_D^{Ma}	0.0201306	$C_D^{Ma\delta_e}$	−0.00383177
C_D^{α}	0.203794	$C_D^{\alpha\delta_e}$	1.98468
$C_D^{\delta_e}$	0.0325529	$C_D^{\alpha^2}$	7.72588
$C_D^{\eta_1}$	0.0025028	$C_D^{\delta_e^2}$	0.945984
$C_D^{\eta_3}$	0.00496105	C_D^{0}	−0.109122
$C_D^{Ma\alpha}$	−0.0241477		

$$
\begin{aligned}
C_M &= C_M^{Ma} Ma + C_M^{\alpha}\alpha + C_M^{\delta_e}\delta_e \\
&\quad + C_M^{\eta_1}\eta_1 + C_M^{\dot{\eta}_2}\dot{\eta}_2 + C_M^{\dot{\eta}_3}\dot{\eta}_3 + C_M^{0}, \\
C_{N_i} &= C_{N_i}^{Ma} Ma + C_{N_i}^{\alpha}\alpha + C_{N_i}^{\delta_e}\delta_e \\
&\quad + C_{N_i}^{\eta_1}\eta_1 + C_{N_i}^{\eta_2}\eta_2 + C_{N_i}^{\eta_3}\eta_3 + C_{N_i}^{0}, \\
&\qquad\qquad i =, 1, 2, 3.
\end{aligned}
\tag{30}
$$

The forces and moments coefficients are all the functions of rigid states, flexible modes, and control inputs, where the lift and general force functions contain linear terms with respect to each variable. Throttle term is omitted in the function of the lift, drag, and general force because of little influence on the fitting accuracy. Adding the cross-terms and higher-order terms can increase the fit accuracy in the drag and thrust functions. The forces and moment contain steady states and unsteady flexible effects.

The fit functions (30) reduce the complexity of the aerodynamic model in Section 2, and the containing of the unsteady flexible effects $\dot{\eta}$ in polynomials reflects the couplings between the flexible structure and aeropropulsion system. The ranges of variables in the fit functions are shown in Table 1, and Tables 2, 3, 4, 5, and 6 show the values of the fit coefficients.

Table 4: The coefficients of fits for the thrust.

Terms	Values	Terms	Values
C_T^{Ma}	0.0059	$C_T^{Ma\phi}$	−126.8976
C_T^{α}	−0.4255	$C_T^{\eta_1}$	132.3165
C_T^{ϕ}	−0.7297	$C_T^{\eta_2}$	−9.3163
$C_T^{\alpha^3\phi}$	0.0081	$C_T^{\eta_3}$	0.1239
$C_T^{\alpha^2\phi}$	0.01	C_T^{0}	−0.0429
$C_T^{\alpha\phi}$	0.0157		

Table 5: The coefficients of fits for the pitching moment.

Terms	Values	Terms	Values
C_M^{Ma}	0.52405	$C_M^{\dot{\eta}_2}$	−0.116657
C_M^{α}	31.7904	$C_M^{\dot{\eta}_3}$	−0.0868456
$C_M^{\delta_e}$	−25.1464	C_M^{0}	−0.887385
$C_M^{\eta_1}$	−0.325935		

Table 6: The coefficients of fits for the generalized forces.

Terms	Values	Terms	Values
$C_{N_1}^{Ma}$	−0.0003	$C_{N_2}^{\eta_1}$	0.0009
$C_{N_1}^{\alpha}$	−0.4515	$C_{N_2}^{\eta_2}$	−0.0012
$C_{N_1}^{\delta_e}$	−0.1517	$C_{N_2}^{\eta_3}$	0.0021
$C_{N_1}^{\eta_1}$	0.0042	$C_{N_2}^{0}$	0.0015
$C_{N_1}^{\eta_2}$	0.001	$C_{N_3}^{Ma}$	0.0005
$C_{N_1}^{\eta_3}$	0.0087	$C_{N_3}^{\alpha}$	−0.1365
$C_{N_1}^{0}$	−0.0027	$C_{N_3}^{\delta_e}$	−0.0527
$C_{N_2}^{Ma}$	−0.0006	$C_{N_3}^{\eta_1}$	0.0009
$C_{N_2}^{\alpha}$	−0.1236	$C_{N_3}^{\eta_2}$	0.0003
$C_{N_2}^{\delta_e}$	−0.0869	$C_{N_3}^{\eta_3}$	0.002
$C_{N_2}^{\delta_c}$	−0.0926	$C_{N_3}^{0}$	−0.0044
$C_{N_2}^{\delta_e}$	−0.0864		

To validate the goodness of the fit functions, we examine the three-dimensional plots of the aerodynamic forces and moments with variables under certain flight conditions. Figures 7 and 8 show the trend of lift and pitching moment with α, δ_e, and Ma; we can see that the trend of the fit curve and the interpolation surface of the experimental data is approximated. The P value is 0, and the coefficient of determination is above 0.9 in the fitting, which shows that the fit functions are very significant. The fitting errors are 0.0672, 0.009, 0.232, 0.0057, 0.0066, 0.0029, and 0.0021, respectively. Then we can conclude that the goodness of the fit is high and the fittings meet the accuracy requirement.

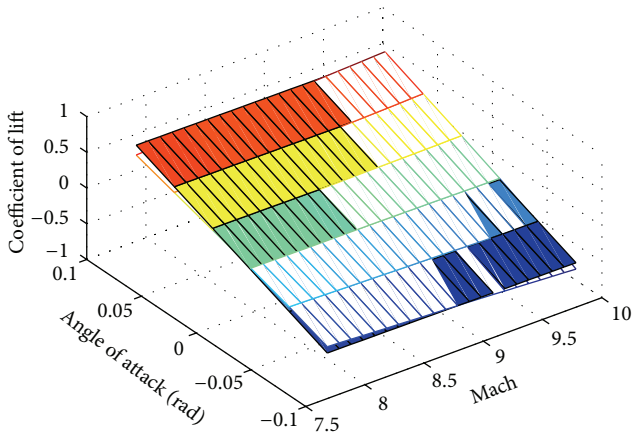

Figure 7: Lift versus α and Ma.

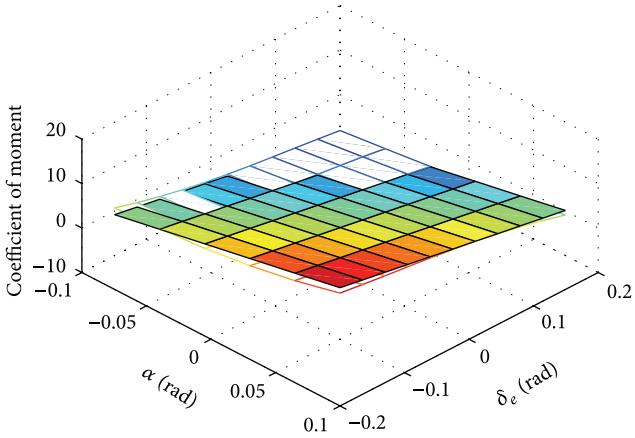

Figure 8: Pitching moment versus α and δ_e.

4. Dynamic Analysis

For the analysis of the dynamic stability, the vehicle is trimmed in steady level flight at an altitude of 85,000 ft and Mach 8; then the vehicle model is linearized at the trim condition in Table 7. The pole-zero map is shown in Figure 9, where the input is the elevator deflection δ_e and the output is the velocity V. We can see that the vehicle has an unstable short period mode, an unstable long period mode, and three stable flexible modes. The flexible modes are pairs of complex conjugate poles and have negative real parts. The RHP zero in Figure 9 shows that the vehicle model is unstable and the nonminimum phase phenomenon exists.

5. Conclusions

Based on the longitudinal geometry of an air-breathing hypersonic vehicle, this work uses the engineering estimated method to calculate the aerodynamics steady forces and moments, viscous effects, and unsteady flexible effects. A physics-based vehicle model which contains aeroflexible structure-propulsion interactions is developed. With the curve fitting approximation method, a simplified control-oriented model is presented, where the forces, moments, and thrust are the polynomial functions of the states and control inputs. The simulations show that the flexible and viscous effects can change the aerodynamic layout on the vehicle and should not be omitted in vehicle modeling. The control-oriented model retains the couplings between the rigid and flexible dynamics and can be applied for controller design.

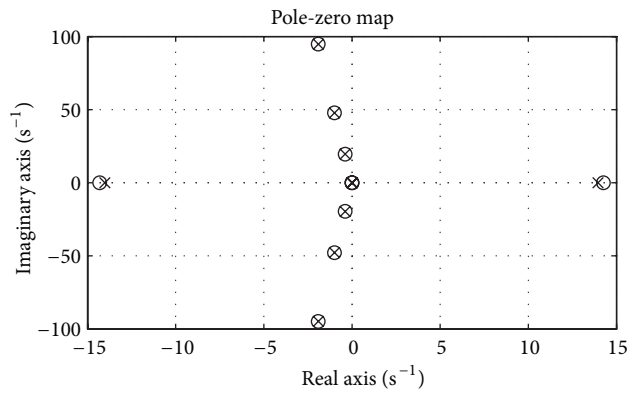

Figure 9: The pole-zero map.

Table 7: Trim at Mach 8,85000 ft height for the model.

States	Value	States	Value
V (Ma)	8	η_3 (ft·slug)	−0.0019934
h (ft)	85000	δ_e (°)	7.9968
α (°)	0.5758	ϕ	0.51914
η_1 (ft·slug)	−0.15266	η_2 (ft·slug)	−0.013716

Conflict of Interests

The authors declare that there is no commercial or associative interest that represents a conflict of interests in connection with the work submitted.

Acknowledgments

This work was supported in part by the National Natural Science Foundation of China under Grant no. 61273092; the Foundation for Key Program of Ministry of Education, China, under Grant no. 311012; Tianjin Basic Research Key Foundation under Grants nos. 11JCZDJC25100, 12JCZDJC30300.

References

[1] J. J. McNamara and P. P. Friedmann, "Aeroelastic and aerothermoelastic analysis of hypersonic vehicles: current status and future trends," in *Proceedings of the 48th AIAA/ASME/ASCE/AHS/ASC Structures, Structural Dynamics, and Materials Conference*, pp. 3814–3868, Honolulu, Hawaii, USA, April 2007.

[2] F. R. Chavez and D. K. Schmidt, "Analytical aeropropulsive/aeroelastic hypersonic-vehicle model with dynamic analysis," *Journal of Guidance, Control, and Dynamics*, vol. 17, no. 6, pp. 1308–1319, 1994.

[3] A. Clark, M. D. Mirmirani, C. Wu, S. Choi, and M. Kuipers, "An aero-propulsion integrated elastic model of a generic airbreathing hypersonic vehicle," in *Proceedings of the AIAA Guidance, Navigation, and Control Conference and Exhibit*, pp. 3699–3718, Keystone, Colo, USA, August 2006.

[4] A. Clark, C. Wu, M. Mirmirani, S. Choi, and M. Kuipers, "Development of an airframe-propulsion integrated generic hypersonic vehicle model," in *Proceedings of the 44th AIAA Aerospace Sciences Meeting and Exhibit*, AIAA 2006-218, pp. 2625–2654, Reno, Nev, USA, January 2006.

[5] M. A. Bolender and D. B. Doman, "Nonlinear longitudinal dynamical model of an air-breathing hypersonic vehicle," *Journal of Spacecraft and Rockets*, vol. 44, no. 2, pp. 374–387, 2007.

[6] M. W. Oppenheimer and D. B. Doman, "A hypersonic vehicle model developed with piston theory," in *Proceedings of the AIAA Atmospheric Flight Mechanics Conference*, AIAA-2006-6637, pp. 1241–1260, Keystone, Colo, USA, August 2006.

[7] M. W. Oppenheimer, T. Skujins, M. A. Bolender, and D. B. Doman, "A flexible hypersonic vehicle model developed with piston theory," in *Proceedings of the AIAA Atmospheric Flight Mechanics Conference and Exhibit*, AIAA 2007-6396, pp. 396–420, Hilton Head Island, SC, USA, August 2007.

[8] J. T. Parker, A. Serrani, S. Yurkovich, M. A. Bolender, and D. B. Doman, "Control-oriented modeling of an air-breathing hypersonic vehicle," *Journal of Guidance, Control, and Dynamics*, vol. 30, no. 3, pp. 856–869, 2007.

[9] L. Fiorentini, A. Serrani, M. A. Bolender, and D. B. Doman, "Nonlinear robust adaptive control of flexible air-breathing hypersonic vehicles," *Journal of Guidance, Control, and Dynamics*, vol. 32, no. 2, pp. 401–416, 2009.

[10] D. O. Sigthorsson and A. Serrani, "Development of linear parameter-varying models of hypersonic air-breathing vehicles," in *Proceedings of the AIAA Guidance, Navigation, and Control Conference and Exhibit*, Chicago, Ill, USA, August 2009.

[11] S. G. V. Frendreis, T. Skujins, and C. E. S. Cesnik, "Six-degree-of-freedom simulation of hypersonic vehicles," in *Proceedings of the AIAA Atmospheric Flight Mechanics Conference*, Chicago, Ill, USA, August 2009.

[12] S. G. V. Frendreis and C. E. S. Cesnik, "3D simulation of flexible hypersonic vehicles," in *Proceedings of the AIAA Atmospheric Flight Mechanics Conference*, Toronto, Canada, August 2010.

[13] J. T. Parker, A. Serrani, S. Yurkovich, M. A. Bolender, and D. B. Doman, "Approximate feedback linearization of an air-breathing hypersonic vehicle," in *Proceedings of the AIAA Guidance, Navigation, and Control Conference and Exhibit*, AIAA 2006-6556, Keystone, Colo, USA, 2006.

[14] H. Li, Y. Si, L. Wu, X. Hu, and H. Gao, "Multi-objective fault-tolerant output tracking control of a flexible air-breathing hypersonic vehicle," *Proceedings of the Institution of Mechanical Engineers I: Journal of Systems and Control Engineering*, vol. 224, no. 6, pp. 647–667, 2010.

[15] H. Li, Y. Si, L. Wu, X. Hu, and H. Gao, "Guaranteed cost control with poles assignment for a flexible air-breathing hypersonic vehicle," *International Journal of Systems Science*, vol. 42, no. 5, pp. 863–876, 2011.

[16] H. Li, L. Wu, H. Gao, X. Hu, and Y. Si, "Reference output tracking control for a flexible air-breathing hypersonic vehicle via output feedback," *Optimal Control Applications and Methods*, vol. 33, no. 4, pp. 461–487, 2012.

[17] Q. Zong, J. Wang, and Y. Tao, "Adaptive high-order dynamic sliding mode control for a flexible air-breathing hypersonic vehicle," *International Journal of Robust and Nonlinear Control*, vol. 23, no. 15, pp. 1718–1736, 2013.

[18] T. Williams, M. A. Bolender, D. B. Doman, and O. Morataya, "An aerothermal flexible mode analysis of a hypersonic vehicle," in *Proceedings of the AIAA Atmospheric Flight Mechanics Conference and Exhibit*, pp. 1391–1412, Keystone, Colo, USA, August 2006.

[19] M. W. Oppenheimer, D. B. Doman, J. J. McNamara, and A. J. Culler, "Viscous effects for a hypersonic vehicle model," in *Proceedings of the AIAA Atmospheric Flight Mechanics Conference and Exhibit*, AIAA 2008-6382, Honolulu, Hawaii, USA, August 2008.

[20] F. Poulain and O. Chatillon, "Nonlinear control of a airbreathing hypersonic vehicle," in *Proceedings of the 16th AIAA/DLR/DGLR International Space Planes and Hypersonic Systems and Technologies Conference*, Bremen, Germany, October 2009.

[21] J. Levin, P. A. Ioannou, and M. D. Mirmirani, "Adaptive mode suppression scheme for an aeroelastic airbreathing hypersonic cruise vehicle," in *Proceedings of the AIAA Guidance, Navigation and Control Conference and Exhibit*, Honolulu, Hawaii, USA, August 2008.

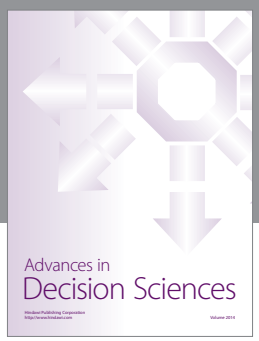

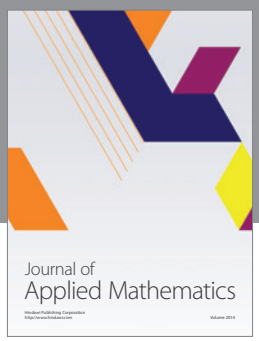

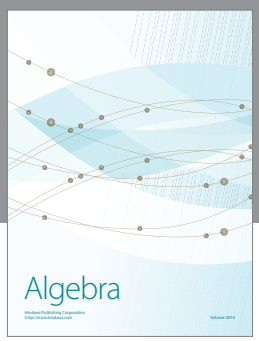

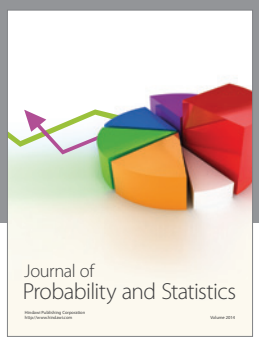

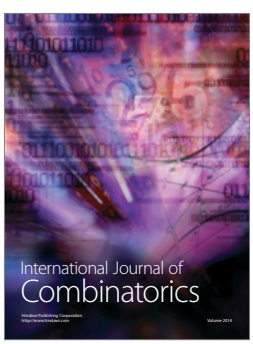

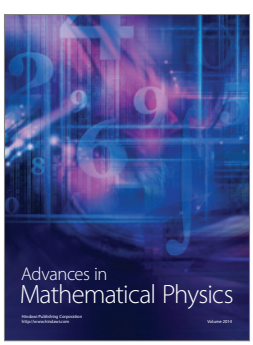

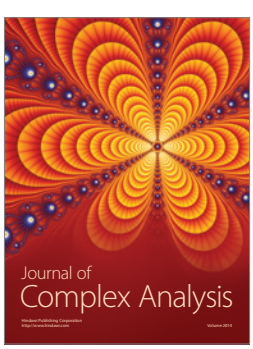

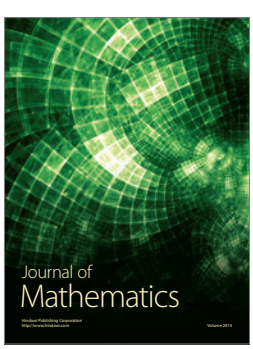

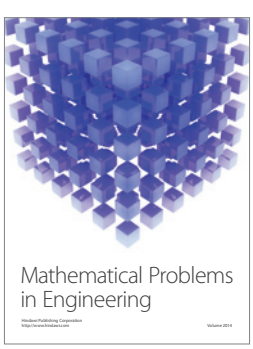

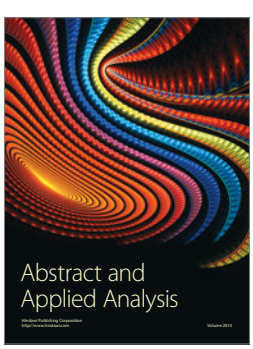

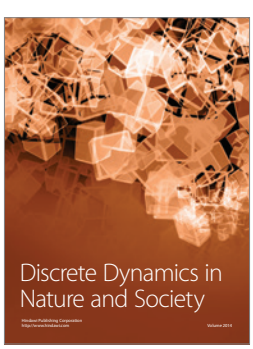

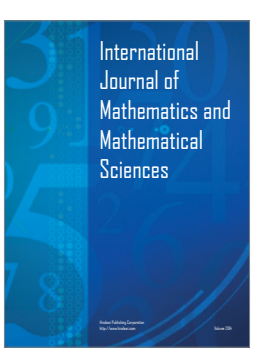

Hindawi

Submit your manuscripts at
http://www.hindawi.com